Smooth control of an articulated mobile robot with switching constraints

doi: 10.1080/01691864.2015.1102646

To appear in *Advanced Robotics*
Vol. 00, No. 00, January 2015, 1–17

FULL PAPER

Smooth Control of an Articulated Mobile Robot with Switching Constraints

Motoyasu Tanaka[a]* , Mizuki Nakajima[a] , and Kazuo Tanaka[a]

[a] *The University of Electro-Communications, 1-5-1 Chofugaoka, Chofu, Tokyo, Japan*;

(*v1.0 released January 2015*)

The paper describes a smooth controller of an articulated mobile robot with switching constraints. The use of switching constraints associated with grounded/lifted wheels is an effective method of controlling various motions; e.g., the avoidance of a moving obstacle. A model of an articulated mobile robot that has active and passive wheels and active joints with switching constraints is derived. A controller that accomplishes the trajectory tracking of the robot's head and sub-tasks using smooth joint input is proposed on the basis of the model. Simulations and experiments are presented to show the effectiveness of the proposed controller.

Keywords: articulated mobile robot; switching constraints; kinematic redundancy; trajectory tracking; snake robot; switched system;

1. Introduction

Articulated mobile robots have several segments serially connected by joints that move adaptively in response to complex environments. Articulated mobile robots are useful for inspecting narrow spaces, such as pipelines and rubble at disaster sites. Many articulated mobile robots [1] have been developed for applications such as the inspection of nuclear reactor sites [2, 3] and pipes [4–7] and search and rescue operations [8–11]. The present paper distinguishes between articulated mobile robots and snake robots according to the locomotive mechanism. A snake robot has active joints and passive wheels, and moves through lateral undulations like a real snake. In contrast, an articulated mobile robot has active joints and a powered mechanism generating a propulsion force in each segment (e.g., an active wheel or a crawler), and moves about without lateral undulations. Articulated mobile robots are more suited to practical situations because propulsion forces are easily generated by a powered mechanism.

There are two well-known methods for the control of articulated mobile robots [1]: the 'follow-the-leader' method and the 'n-trailer' method. In the follow-the-leader method, the motion of the head (leader) is determined first, and the motion sequentially shifts to the trailing segments (the followers). The method is used in the control of KR-II[3], GMD-SNAKE2[5], MAKRO[6], and ACM–R4[12]. Moreover, ACM–R4.1[13] and R4.2[14] actively accomplish motion by maintaining all wheels on the ground, even on uneven terrain, using a torque sensor based on the method.

In the n-trailer method, the robot is steered by treating the motion of the whole body of the robot as that of a truck (the head segment) pulling connected trailers (following segments) behind it. If the motion of the head is given, the motion of the following segments is passively determined according to the kinematics of the problem, meaning that the wheels do not slide

*Corresponding author. Email: mtanaka@uec.ac.jp

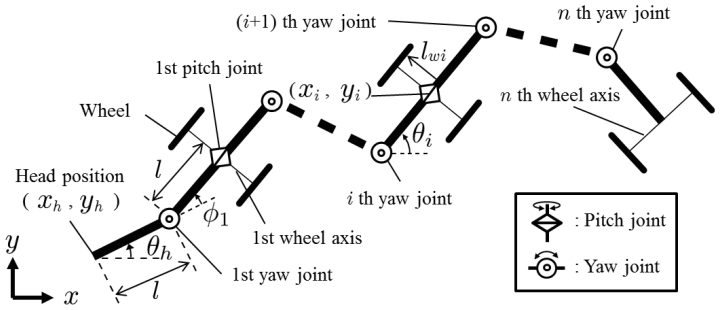

Figure 1. Articulated mobile robot.

sideways. KOHGA [11], which has active/passive joints and crawlers, and an articulated mobile robot [15], which has active joints and active wheels, are controlled using this method.

Using either method, the motion of the following segments is determined according to the shift or kinematics that depend on the motion of the head. It is thus difficult to change directly the motion of parts of the robot other than the head.

We have proposed a control method [16] by which the head of the snake robot tracks the desired trajectory and the body shape of the robot is freely determined at some level using mode switching of the grounded parts of the body. The kinematic model of the robot is derived using the velocity constraints dictated by the grounded wheels. Thus, mode switching of the grounded/lifted wheels of the robot implies switching constraints. Employing the method, a snake robot can accomplish several tasks that were impossible when employing previous methods, in particular, avoiding moving obstacles [16], approximating path trajectories of the joints of the snake robot [17], and performing semi-autonomous whole-body collision avoidance based on range sensors [18]. It is possible for an articulated mobile robot to accomplish the same tasks by applying this control method, as the method allows the robot to change body shape adaptively during locomotion. However, the method in [16–18] is problematic in that the angular velocity input from the joint jumps depending on the switching mode of the grounded/lifted wheel. The jump is unwanted when determining the joint torque needed to achieve a certain angular velocity.

Smoothing is necessary to prevent the jump in input. In robotics, a popular method for smoothing is to use filters. The method smoothly shapes the input using a filter and is effective in preventing residual vibration [19, 20]. Another method is to use approximate curves, and is used for the path planning of mobile robots [21–23]. However, these two methods reshape the input without considering the mathematical model of the controlled robot. If these methods are applied to the input of [16–18], trajectory tracking for the reference and several subtasks cannot be ensured.

This paper describes a smooth controller for an articulated mobile robot with switching constraints. First, a model of the robot considering mode switching of the wheels is derived and a control method for the robot with switching constraints is proposed. The proposed method accomplishes several tasks; e.g., trajectory tracking of the robot's head and avoidance of a moving obstacle. Moreover, the proposed method prevents any jump in the angular velocity input, the main problem relating to previous work [16–18], and generates a smooth input. Simulations and experiments showing the effectiveness of the proposed controller are presented.

2. Model

This section describes the mechanics of an articulated mobile robot, which is the controlled object in this study, and derives a kinematic model for the robot (Figure 1). The robot has n segments, each comprising a pitch rotational joint, a yaw rotational joint, and a pair of wheels. The pitch rotational joint and the pair of wheels are coaxially mounted. All joints are active and

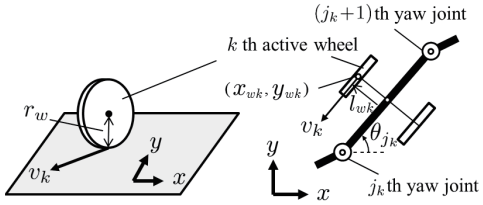

Figure 2. Position and velocity variables for an active wheel.

each wheel is either active or passive. If all wheels are passive, the robot is equivalent to that in [16–18].

As indicated in Figure 1, let l be the length of a link, n the number of yaw joints and wheel axes, $\boldsymbol{w} = [x_h, y_h, \theta_h]^T$ the position and attitude of the robot's head, ϕ_i the i-th yaw angle, and (x_i, y_i) the position of the point of intersection of the i-th wheel axis and the link. We set $\boldsymbol{\phi} = [\phi_1, \cdots, \phi_n]^T$ and $\boldsymbol{\theta} = [\theta_h, \boldsymbol{\phi}^T]^T$. We assume that the wheel does not slip sideways. Then, the velocity constraint is represented as

$$\dot{x}_i \sin\theta_i - \dot{y}_i \cos\theta_i = 0, \tag{1}$$

where $\theta_i = \theta_h + \sum_{j=1}^{i} \phi_j$.

Next, we consider the velocity constraint required for the active wheels. Here the maximum number of active wheels attached to each wheel axis is two. Let $n_w (0 \leq n_w \leq 2n)$ be the total number of active wheels, ρ_k the rotation angle of the k-th active wheel, j_k the index of the wheel axis where the k-th active wheel is attached, (x_{wk}, y_{wk}) the position where the k-th active wheel touches the ground, and r_w the radius of each wheel. We set $\boldsymbol{\rho} = [\rho_1, \cdots, \rho_{n_w}]^T$ and $\boldsymbol{q} = [\boldsymbol{w}^T, \boldsymbol{\phi}^T, \boldsymbol{\rho}^T]^T$. We assume that the k-th active wheel does not slip to the direction of v_k. Then, from Figure 2, it follows that

$$\dot{x}_{wk} \cos\theta_{j_k} + \dot{y}_{wk} \sin\theta_{j_k} = -v_k = -r_w \dot{\rho}_k. \tag{2}$$

Here, we set $\boldsymbol{u} = [\dot{\boldsymbol{\phi}}^T, \dot{\boldsymbol{\rho}}^T]^T$. By arranging (1) and (2), it follows that

$$\boldsymbol{A}_a(\boldsymbol{\theta})\dot{\boldsymbol{w}} = \boldsymbol{B}_a(\boldsymbol{\theta})\boldsymbol{u}, \tag{3}$$

$$\boldsymbol{A}_b(\boldsymbol{\theta})\dot{\boldsymbol{w}} = \boldsymbol{B}_b(\boldsymbol{\theta})\boldsymbol{u}, \tag{4}$$

where $\boldsymbol{A_a} \in \mathbf{R}^{n\times 3}$, $\boldsymbol{B_a} \in \mathbf{R}^{n\times(n+n_w)}$, $\boldsymbol{A_b} \in \mathbf{R}^{n_w\times 3}$, and $\boldsymbol{B_b} \in \mathbf{R}^{n_w\times(n+n_w)}$. Let a_{ij} be the element of the i-th row and j-th column of $\boldsymbol{A}_a$, b_{kj} be the element of the k-th row and j-th column of $\boldsymbol{A}_b$, and l_{wk} be the length related to the position of the k-th active wheel, as illustrated in Figure 2.

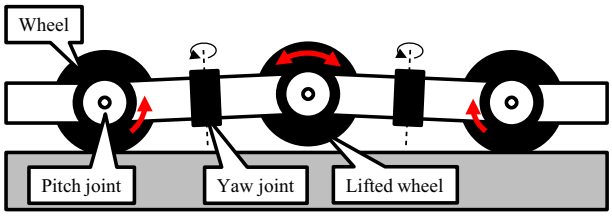

Figure 3. Pitch joint angles and lifted wheels.

Then a_{ij} and b_{kj} are obtained as

$$a_{i1} = \sin\theta_i, \tag{5}$$

$$a_{i2} = -\cos\theta_i, \tag{6}$$

$$a_{i3} = -l\{1 + \cos(\theta_i - \theta_h) + 2\sum_{s=1}^{i-1}\cos(\theta_i - \theta_s)\}, \tag{7}$$

$$b_{k1} = \cos\theta_{j_k}, \tag{8}$$

$$b_{k2} = \sin\theta_{j_k}, \tag{9}$$

$$b_{k3} = -l_{wk} + l\{1 + \sin(\theta_{j_k} - \theta_h) + 2\sum_{s=1}^{j_k-1}\sin(\theta_{j_k} - \theta_s)\}. \tag{10}$$

The i-th row of (3) corresponds to (1) related to the i-th wheel axis, and the k-th row of (4) corresponds to (2) related to the k-th active wheel. Thus, if all wheels are grounded, the velocity constraint of the articulated mobile robot is represented as

$$\boldsymbol{A}(\boldsymbol{\theta})\dot{\boldsymbol{w}} = \boldsymbol{B}(\boldsymbol{\theta})\boldsymbol{u}, \tag{11}$$

$$\boldsymbol{A} = \begin{bmatrix} A_a \\ A_b \end{bmatrix}, \quad \boldsymbol{B} = \begin{bmatrix} B_a \\ B_b \end{bmatrix} = \begin{bmatrix} l & 0 & & \cdots & & 0 \\ * & \ddots & \ddots & & & \\ & \ddots & l & 0 & & \vdots \\ \vdots & & * & -r_w & \ddots & \\ & & & \ddots & \ddots & 0 \\ * & & \cdots & & * & -r_w \end{bmatrix}, \tag{12}$$

where $\boldsymbol{A} \in \mathbf{R}^{(n+n_w)\times 3}$, $\boldsymbol{B} \in \mathbf{R}^{(n+n_w)\times(n+n_w)}$, and '$*$' signifies nondiagonal elements; their detailed description is omitted. $\boldsymbol{B}$ is always invertible because it is a lower-triangular matrix and its diagonal elements are non-zero constant.

2.1 *Kinematic model introducing switching constraints*

We describe the switching of the wheel status from grounded to lifted and vice versa [16–18] for our articulated mobile robot. While the wheels are necessary for the robot to move, they sometimes limit the robot's mobility. For example, when all wheels are grounded and a moving obstacle approaches the body of the robot from the side, the velocity constraint restraining sideways movements prevents any movement to avoid a collision. If the robot could make a wheel slip sideways by exerting a large force, it could then perform an evasive motion. However,

in this instance, a large torque from the joints is needed. In contrast, if the robot was able to lift a wheel, it could then perform an evasive motion without a large torque as the velocity constraint disappears.

The articulated mobile robot can switch the grounded/lifted status of wheels by varying the angle of the pitch joint in a manner similar to that of the snake robot described in [16–18]. The robot could switch its status for each wheel axis by rotating the pitch joints slightly, as depicted in Figure 3. In the present paper, the pitch joints are only used for switching the status for each wheel axis. Thus, we assume that the magnitude of the pitch angle is very small and the motion of the pitch joints in the xy-plane does not affect the motion of the robot.

The model of the robot also switches depending on the grounded/lifted status of the wheel axes. We allocate a unique index, which is called the 'mode', to each model to represent the overall status of the wheel axes. Let σ be the discrete mode number where the i-th wheel axis ($i = i_1, \cdots, i_{m_\sigma}$) and j-th active wheel ($j = j_1, \cdots, j_{a_\sigma}$) are lifted. In this instance, the i-th row in (3) and j-th row in (4) disappear. Thus, (11) becomes

$$\boldsymbol{A}_\sigma \dot{\boldsymbol{w}} = \boldsymbol{B}_\sigma \boldsymbol{u}, \tag{13}$$

$$\boldsymbol{A}_\sigma = \begin{bmatrix} \boldsymbol{A}_{a\sigma} \\ \boldsymbol{A}_{b\sigma} \end{bmatrix}, \quad \boldsymbol{B}_\sigma = \begin{bmatrix} \boldsymbol{B}_{a\sigma} \\ \boldsymbol{B}_{b\sigma} \end{bmatrix}, \tag{14}$$

where $\boldsymbol{A}_\sigma \in \mathbf{R}^{(n+n_w-m_\sigma-a_\sigma)\times 3}$, $\boldsymbol{B}_\sigma \in \mathbf{R}^{(n+n_w-m_\sigma-a_\sigma)\times(n+n_w)}$, $\boldsymbol{A}_{a\sigma} \in \mathbf{R}^{(n-m_\sigma)\times 3}$, $\boldsymbol{A}_{b\sigma} \in \mathbf{R}^{(n_w-a_\sigma)\times 3}$, $\boldsymbol{B}_{a\sigma} \in \mathbf{R}^{(n-m_\sigma)\times(n+n_w)}$, and $\boldsymbol{B}_{b\sigma} \in \mathbf{R}^{(n_w-a_\sigma)\times(n+n_w)}$. $\boldsymbol{A}_{a\sigma}$ and $\boldsymbol{B}_{a\sigma}$ denote the matrices for which the i-th row from $\boldsymbol{A}_a$ and $\boldsymbol{B}_a$, respectively, are removed. Similarly, $\boldsymbol{A}_{b\sigma}$ and $\boldsymbol{B}_{b\sigma}$ denote the matrices for which the j-th row from $\boldsymbol{A}_b$ and $\boldsymbol{B}_b$, respectively, are removed. $\boldsymbol{A}_\sigma$ and $\boldsymbol{B}_\sigma$ can be represented as

$$\boldsymbol{A}_\sigma = \boldsymbol{T}_\sigma \boldsymbol{A}, \quad \boldsymbol{B}_\sigma = \boldsymbol{T}_\sigma \boldsymbol{B}, \tag{15}$$

where $\boldsymbol{T}_\sigma \in \mathbf{R}^{(n+n_w-m_\sigma-a_\sigma)\times(n+n_w)}$ is a selection matrix for which the elements are either 0 or 1. $\boldsymbol{T}_\sigma$ is the matrix obtained by removing the i-th row and the $n+j$-th row from the identity matrix $\boldsymbol{I}$.

Let ΔT be the switching time period of the mode. The kinematic model of the articulated mobile robot with switching constraints is expressed as

$$\begin{aligned} \boldsymbol{A}_\sigma \dot{\boldsymbol{w}} &= \boldsymbol{B}_\sigma \boldsymbol{u}, \\ \sigma(t) &= \sigma_k, \quad \forall t \in [t_k, t_{k+1}) \end{aligned} \tag{16}$$

where $\sigma \in M$ is the discrete mode number, $M = \{1, 2, \cdots, N_m\}$, N_m is the total number of modes, and $t_k = k\Delta T (k = 0, 1, 2, \cdots)$ is the switching time. The robot switches at time t_k, and the mode is maintained over the interval $t_k \le t < t_{k+1}$. If $n_w = 0$, the model is equivalent to the model in [16–18].

3. Controller design

In the realization of the desired trajectory of the head of a snake robot, the angular velocity is not unique when some of the wheels are lifted off the ground. The feature is called kinematic redundancy (redundancy II in [24]). Moreover, various tasks (e.g., avoidance of a moving obstacle) were accomplished using both kinematic redundancy and mode selection in [16–18]. The articulated mobile robot in the present study also has kinematic redundancy and can switch modes. This section presents and describes the control method using both kinematic redundancy and mode selection.

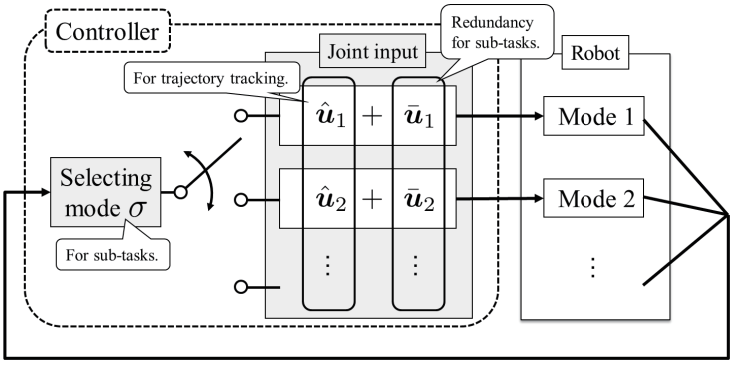

(a) Previous method [16–18]

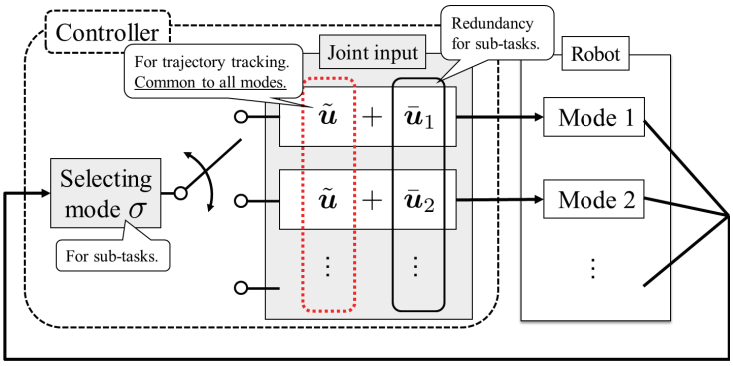

(b) Proposed method

Figure 4. Control systems.

The main control objective, alternatively called the main task, is to verify that the position and attitude of the head track the desired trajectory. The sub-task is any additional control objective that the robot should accomplish besides the main task. We define the cost function $V(\boldsymbol{q})$, and assume that the robot accomplishes the sub-task by decreasing V.

In this paper, an improved method that suppresses jumps in the joint input, the problem with the previous method [16–18], is proposed.

3.1 *Previous method of [16–18] and its problem*

Figure 4(a) sketches the algorithm of the previous controller described in [16–18]. The controller consists of a part calculating joint inputs and a part selecting modes. The former provides the different joint input for each mode. The joint input consists of $\hat{\boldsymbol{u}}_\sigma$ depending on the main task and $\bar{\boldsymbol{u}}_\sigma$ depending on the sub-task. The latter selects the optimal mode considering the effect for the sub-task. The robot can accomplish both the main task and sub-task using the controller. In particular, the advantage of the method is its practicality in advanced tasks [16–18] that cannot be performed without mode switching. Different uses of kinematic redundancy and the method in selecting modes is exploited in [16–18] because of the differences in each sub-task.

In applying the controller of the previous work [16] to an articulated mobile robot, the joint

input is represented as

$$\boldsymbol{u}(t) = \hat{\boldsymbol{u}}_\sigma + \bar{\boldsymbol{u}}_\sigma, \tag{17}$$

$$\hat{\boldsymbol{u}}_\sigma = \boldsymbol{B}_\sigma^\dagger \boldsymbol{A}_\sigma \{\dot{\boldsymbol{w}}_d - \boldsymbol{K}(\boldsymbol{w} - \boldsymbol{w}_d)\}, \tag{18}$$

$$\bar{\boldsymbol{u}}_\sigma = \kappa(\boldsymbol{I} - \boldsymbol{B}_\sigma^\dagger \boldsymbol{B}_\sigma)\boldsymbol{\eta}, \tag{19}$$

$$\boldsymbol{\eta} = \left[\frac{\partial V}{\partial \phi_1}, \cdots, \frac{\partial V}{\partial \phi_n}, \ \frac{\partial V}{\partial \rho_1}, \cdots, \frac{\partial V}{\partial \rho_{n_w}}\right]^T \in \mathbf{R}^{(n+n_w)}, \tag{20}$$

where $\boldsymbol{w}_d$ is a desired vector of $\boldsymbol{w}$, $\boldsymbol{K} > \boldsymbol{0}$ a feedback gain for the main task, $\boldsymbol{B}_\sigma^\dagger$ a pseudo-inverse matrix of $\boldsymbol{B}_\sigma$, and κ a gain for the sub-task. In (17), $\hat{\boldsymbol{u}}_\sigma$ is an element for the main task and $\bar{\boldsymbol{u}}_\sigma$ is an element representing kinematic redundancy. If all wheels are grounded, $\boldsymbol{B}_\sigma$ becomes a square matrix and $\bar{\boldsymbol{u}}_\sigma$ disappears.

Using (17), the control variable tracks the desired trajectory and (19) assesses the accomplishment of the sub-task [16]. However, there is a problem that (17) generates jumps in the joint input during mode switching because the joint input is different with respect to each mode. The jump is also generated in models described in [17, 18].

We propose an improved control method that prevents jumps in the joint input during mode switching and generates smooth input. Figure 4(b) shows the controller proposed in this paper. The proposed method has a different joint input from Figure 4(a).

3.2 *Smooth joint input*

The jump in (17) is caused by $\hat{\boldsymbol{u}}_\sigma$ being dependent on the main task and $\bar{\boldsymbol{u}}_\sigma$ being related to kinematic redundancy. Thus, the two inputs from the main task and kinematic redundancy are modified to prevent the jump.

3.2.1 Input for main task

The joint input is modified as

$$\boldsymbol{u}(t) = \tilde{\boldsymbol{u}} + \bar{\boldsymbol{u}}_\sigma, \tag{21}$$

$$\tilde{\boldsymbol{u}} = \boldsymbol{B}^{-1}\boldsymbol{A}\{\dot{\boldsymbol{w}}_d - \boldsymbol{K}(\boldsymbol{w} - \boldsymbol{w}_d)\}. \tag{22}$$

The difference between (21) and (17) is the first term on the right-hand side, which is the element depending on the main task. Substituting (21) into (16) and considering (15) and $\boldsymbol{B}_\sigma \bar{\boldsymbol{u}}_\sigma = \boldsymbol{0}$, the closed-loop system is expressed as

$$\begin{aligned} &\boldsymbol{A}_\sigma \dot{\boldsymbol{w}} = \boldsymbol{B}_\sigma \boldsymbol{B}^{-1}\boldsymbol{A}\{\dot{\boldsymbol{w}}_d - \boldsymbol{K}(\boldsymbol{w} - \boldsymbol{w}_d)\}, \\ &\Rightarrow \boldsymbol{A}_\sigma \dot{\boldsymbol{w}} = \boldsymbol{T}_\sigma \boldsymbol{B}\boldsymbol{B}^{-1}\boldsymbol{A}\{\dot{\boldsymbol{w}}_d - \boldsymbol{K}(\boldsymbol{w} - \boldsymbol{w}_d)\}, \\ &\Rightarrow \boldsymbol{A}_\sigma\{\dot{\boldsymbol{w}} - \dot{\boldsymbol{w}}_d + \boldsymbol{K}(\boldsymbol{w} - \boldsymbol{w}_d)\} = \boldsymbol{0}. \end{aligned} \tag{23}$$

Thus, if $\boldsymbol{A}_\sigma$ is of full column rank, $\boldsymbol{w} \to \boldsymbol{w}_d$ is concluded at $t \to \infty$. If $\boldsymbol{A}_\sigma$ is not of full column rank, the convergence of $\boldsymbol{w}$ is not guaranteed because $\dot{\boldsymbol{w}} - \dot{\boldsymbol{w}}_d + \boldsymbol{K}(\boldsymbol{w} - \boldsymbol{w}_d) = \boldsymbol{0}$ does not necessarily hold. This implies that the robot is in a singular configuration. From (23), the size of $\boldsymbol{A}_\sigma$ is also related to whether the controlled variable can be controlled. If $(n + n_w - m_\sigma - a_\sigma) < 3$ which implies that the length of the row is larger than the length of the column in $\boldsymbol{A}_\sigma$, $\boldsymbol{w}$ cannot converge to $\boldsymbol{w}_d$ because $\boldsymbol{A}_\sigma$ is not of full column rank. Thus, it is necessary to satisfy the inequality

$$(n + n_w - m_\sigma - a_\sigma) \geq 3. \tag{24}$$

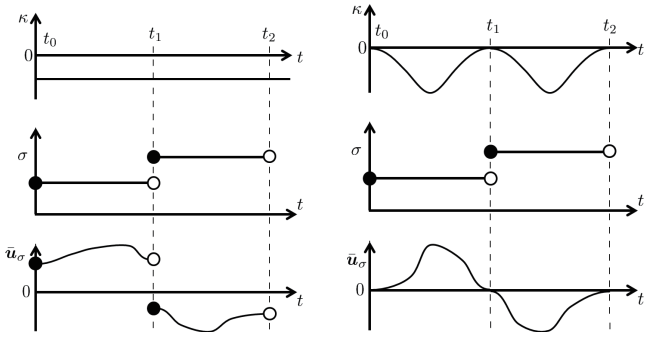

(a) κ =const. (b) $\kappa(t_k) = 0$

Figure 5. Relationship between κ and $\bar{\boldsymbol{u}}_\sigma$

$\hat{\boldsymbol{u}}_\sigma$ in (17) can accomplish the main task in mode σ only. In contrast, $\tilde{\boldsymbol{u}}$ in (21) is calculated assuming that all wheels are grounded, and is a constrained input that can accomplish the main task in all modes ($\sigma = 1, \cdots, N_m$). Using (21), the element for the main task in the input is common to all modes. Therefore, the jump in input depending on the main task is not generated.

3.2.2 Number of modes N_m

A method used to calculate the number of modes N_m when all wheels are passive ($n_w = 0$) was proposed in [16]. This subsection presents a method of calculating N_m when wheels are active ($n_w \neq 0$).

We consider the case that each wheel axis has one active wheel; i.e., $n_w = n, a_\sigma = m_\sigma$. From (24), the robot kinematics has to satisfy $2n - 2m_\sigma \geq 3$. Thus, the maximum number of m_σ is $(n-2)$ and at least two wheel axes must each have a grounded wheel. The robot can elect which wheel axes are to have a grounded wheel. The total number of combinations in this scenario is 2^n. By subtracting the number of combinations for which the number of axes having grounded wheels is less than two, the total number of modes N_m of the robot is obtained from

$$N_m = 2^n - (n+1) \tag{25}$$

where $(n+1)$ is the number of combinations for which one axis has a grounded wheel plus all wheel axes are lifted. For example, $N_m = 26$ if $n = 5$, and $N_m = 247$ if $n = 8$.

Next, we consider each wheel axis has two active wheels, i.e., $n_w = 2n, a_\sigma = 2m_\sigma$. From (24), the robot kinematics has to satisfy $3n - 3m_\sigma \geq 3$ and at least one axis has a grounded wheel. In this case, N_m is $N_m = 2^n - 1$.

If each wheel axis has a different number of active wheels, N_m cannot be calculated as described above, because the minimum number of wheel axes with grounded wheels is not constant; i.e., the minimum number is one, two, or three. In this case, N_m should be counted by checking whether (24) is satisfied for all combinations of grounded wheels.

3.3 *Input related to redundancy*

By considering (19), (20), and (21), $\dot{V}$ is obtained as

$$\begin{aligned}\dot{V}(\boldsymbol{q}) &= \frac{\partial V}{\partial \boldsymbol{w}}\dot{\boldsymbol{w}} + \left[\frac{\partial V}{\partial \boldsymbol{\phi}},\ \frac{\partial V}{\partial \boldsymbol{\rho}}\right]\boldsymbol{u} \\ &= \frac{\partial V}{\partial \boldsymbol{w}}\dot{\boldsymbol{w}} + \boldsymbol{\eta}^T\tilde{\boldsymbol{u}} + \kappa\boldsymbol{\eta}^T(\boldsymbol{I} - \boldsymbol{B}_\sigma^\dagger\boldsymbol{B}_\sigma)\boldsymbol{\eta},\end{aligned} \tag{26}$$

where the first and second terms on the right-hand side depend on the main task, and the third term is related to kinematic redundancy. If $\kappa < 0$, the third term on the right-hand side contributes by decreasing V because $(\boldsymbol{I} - \boldsymbol{B}_\sigma^\dagger \boldsymbol{B}_\sigma) \geq 0$ [25].

In (21), $\tilde{\boldsymbol{u}}$ does not depend on σ but $\bar{\boldsymbol{u}}_\sigma$ is different in each mode. It is possible that the large jump in the joint input is generated by $\bar{\boldsymbol{u}}_\sigma$ on each switching, as shown in Figure 5(a). Thus, we choose κ to be a smooth function that becomes zero ($\kappa = 0$) at switching times t_k ($k = 0, 1, \cdots$), as shown in Figure 5(b). As a result, $\bar{\boldsymbol{u}}_\sigma = \boldsymbol{0}$ is satisfied at t_k and the $\bar{\boldsymbol{u}}_\sigma$-dependent jump in the input does not arise. The joint input at the switching time is smoothly connected using (21) and setting κ as in Figure 5(b). In contrast, from (26), the element related to kinematic redundancy does not contribute to decreasing V if $\kappa = 0$. However, it is sufficient to decrease V by setting the shape and the maximum value of κ because $\kappa < 0$ at $t \neq t_k$.

3.4 *Mode selection*

In previous work [16–18], mode selection was performed with different formulations because of differences in sub-tasks. This section presents a formulation of mode selection that covers also those of [16–18].

The mode $\sigma = \sigma_k$ selected at $t = t_k$ is maintained over the interval $t_k \leq t < t_{k+1}$. Therefore, the robot must predict the mode that is suitable for the robot's motion for this interval. This problem resembles model-predictive control [26, 27], which determines a control input for some future finite-time interval. Therefore, the mode selection is formulated as the optimal problem obtaining the optimal mode $\sigma = \sigma_k$ that minimizes the following J at $t = t_k$.

$$\min_{\sigma_k} \quad J, \tag{27}$$

where

$$J = \varphi(\hat{\boldsymbol{q}}(t_{k+1}, \sigma_k)) + \int_{t_k}^{t_{k+1}} \Gamma(\hat{\boldsymbol{q}}(\tau, \sigma_k), \boldsymbol{u}(\tau, \sigma_k)) d\tau \tag{28}$$

and φ and Γ are functions related to sub-tasks considered in the mode selection. Here φ only depends on the termination value of the prediction period $t = t_{k+1}$, whereas Γ depends on times within the prediction period, $t_k \leq t \leq t_{k+1}$. φ and Γ should be appropriately set depending on the nature of the sub-tasks. For example, we set $\varphi = 0$ and $\Gamma = V$ in [16, 18], and $\varphi = V$ and $\Gamma = 0$ in [17]. In (28), $\hat{\boldsymbol{q}}(t, \sigma)$ is the estimated vector of $\boldsymbol{q}$ at time t when the mode is σ, and is calculated by numerically integrating (23) and (21). (27) is numerically solved by comparing J calculated for all modes, and the obtained mode σ_k is used at $t_k \leq t < t_{k+1}$. Moreover, we use two conditions proposed in [16] as constraints on (27). One ensures the static stability of the motion for walking robots, and the other prevents switching that is impractical. The term statically stable means that the center of gravity of the robot is contained in the supporting polygon constructed from the contact points of the grounded wheels. Details of these conditions are omitted (see [16] or [17]).

Note that the robot sometimes actually becomes statically unstable because $\hat{\boldsymbol{q}}$ in (28) is the estimated vector. In this case, the robot can remain statically stable by grounding some of its wheels until a stable mode is reached. In this study, if the robot becomes statically unstable, we ensure its static stability by grounding all wheels simultaneously.

4. Simulations

Simulations were performed to demonstrate the effectiveness of the proposed control method. We use the articulated mobile robot, as depicted in Figure 6. In the robot, all wheel axes have

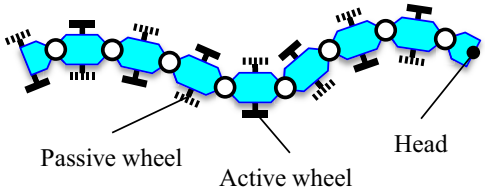

Figure 6. Model of simulations.

one active wheel and the active wheels alternate from one side to the other along the body. In this case, $n = 8$, $n_w = 8$, and $N_m = 247$ from (25).

4.1 *Cost function*

One of the effective sub-tasks that a snake robot can accomplish using mode switching is the avoidance of moving obstacles [16]. The same sub-task can be accomplished for an articulated mobile robot with active wheels. Therefore, we set this avoidance problem as a sub-task. Let (x_i, y_i) be the position of the intersection point of the i-th wheel axis and the link, (x_{ob}, y_{ob}) be the position of the obstacle, and d_i be the distance between (x_i, y_i) and (x_{ob}, y_{ob}). Let us define the cost function V and functions φ and Γ related to switching:

$$V(\boldsymbol{q}) = \sum_{i=1}^{n} \frac{1}{d_i}, \tag{29}$$

$$\varphi = 0, \ \Gamma = V. \tag{30}$$

Using (21) and (27), V decreases and d_i increases. As a result, the risk of collision between the robot and obstacle can be reduced.

There have never been instances in simulations and experiments where $\boldsymbol{A}_\sigma$ is rank deficient, as we shall discussed below. Hence, this study does not consider the avoidance of singular configurations as one of the sub-tasks.

4.2 *Simulation results*

We set $\boldsymbol{w}_d = [0.01t, 0, \pi]^T$, $\boldsymbol{K} = \boldsymbol{I}$, $\Delta T = 1$, and $(x_{ob}, y_{ob}) = (-0.3, 0.01t - 0.1)$. Figure 7 shows the results when the previous input (17) and $\kappa = -1$ (fixed value) are used. κ was heuristically determined by simulations. The pink-colored segments of the robot represent axes with lifted wheels. d_{min} is the minimum value of d_i, which is the distance between (x_i, y_i) and (x_{ob}, y_{ob}). We use $s = \delta_{min}/\delta_{max}$ as a measure of singularity, where δ_{min} and δ_{max} are the minimum and maximum singular values of $\boldsymbol{A}_\sigma$, respectively. If $\boldsymbol{A}_\sigma$ is rank deficient, s becomes zero. From Figure 7(a)–(c), it is seen that the head of the robot tracked the desired trajectory and the whole body of the robot avoided the obstacle by switching modes. The robot avoided singular configurations because $s \neq 0$. However, from Figure 7(d) and (e), it is seen that a jump in the input was generated many times. In particular, the jump in $\dot{\boldsymbol{\rho}}$ was large because it became zero when the corresponding axis had lifted wheels. For a real robot, this jump in joint input is undesirable because a large torque is needed to generate an angular velocity at the joint.

In contrast, Figure 8 shows the results when the proposed smooth input (21) and $\kappa = \{\cos(2\pi t/\Delta T) - 1\}$ are used. The robot accomplished both the main task and sub-task, and avoided singular configurations because of $s \neq 0$. Moreover, the jump in input was smoother, showing better control; see Figure 8(d) and (e).

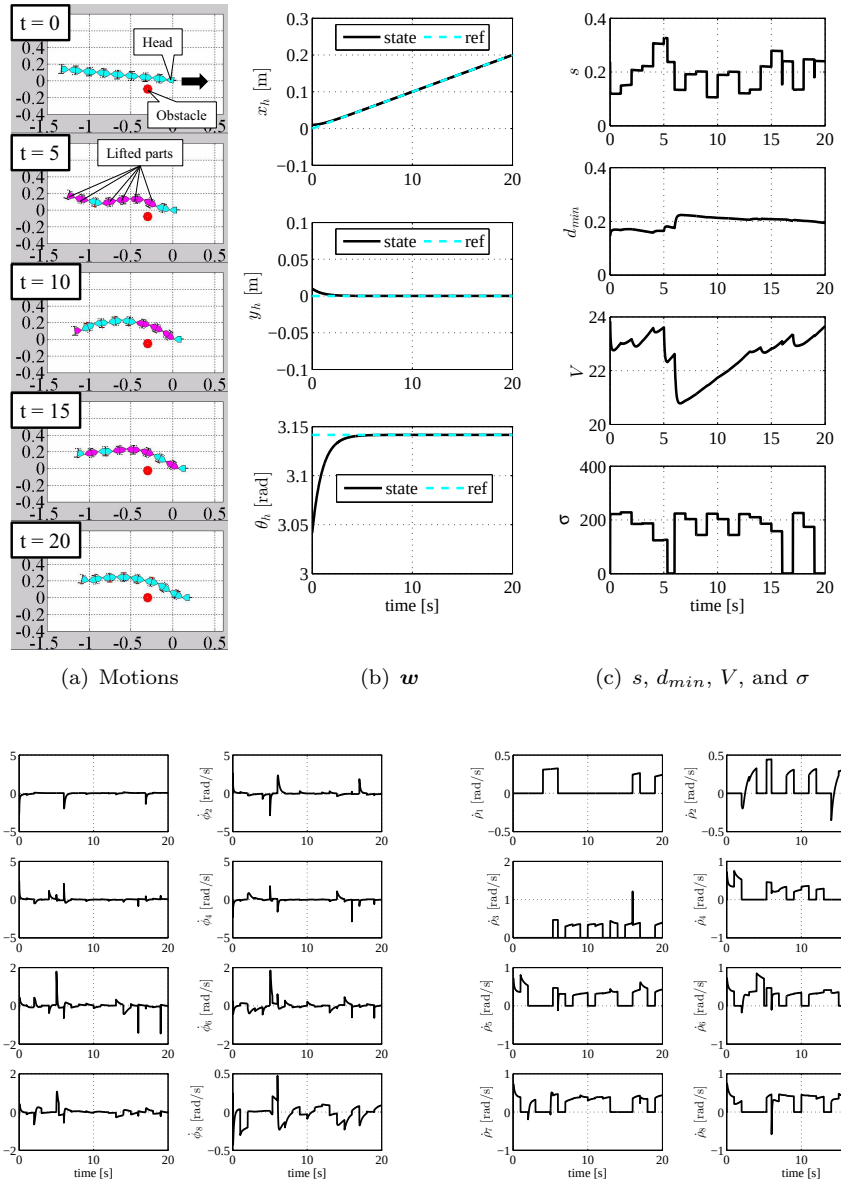

(a) Motions (b) $\boldsymbol{w}$ (c) s, d_{min}, V, and σ

(d) $\dot{\boldsymbol{\phi}}$ (e) $\dot{\rho}$

Figure 7. Simulation results obtained without using the smooth controller.

4.3 *Mode reduction*

For $n = 8$, the number of modes is large and real-time control of an actual robot is difficult because of the associated large calculation costs in deriving solutions (27). Moreover, lifting many adjacent links (e.g., four adjacent wheel axes are lifted at $t = 5$ s in Figure 7(a)) is difficult for an actual robot because large torques must be generated by the actuators of the pitch joints. Similar to [18], we reduced the number of modes to eight, as shown in Figure 9, solely to decrease the calculation cost and to avoid insufficient torque. Figure 10 shows the results obtained by reducing the number of modes. Because of this difference in the number of modes, the avoidance motion in Figure 10(a) is different from that in Figure 8(a). Nevertheless, the robot avoided collisions in both cases.

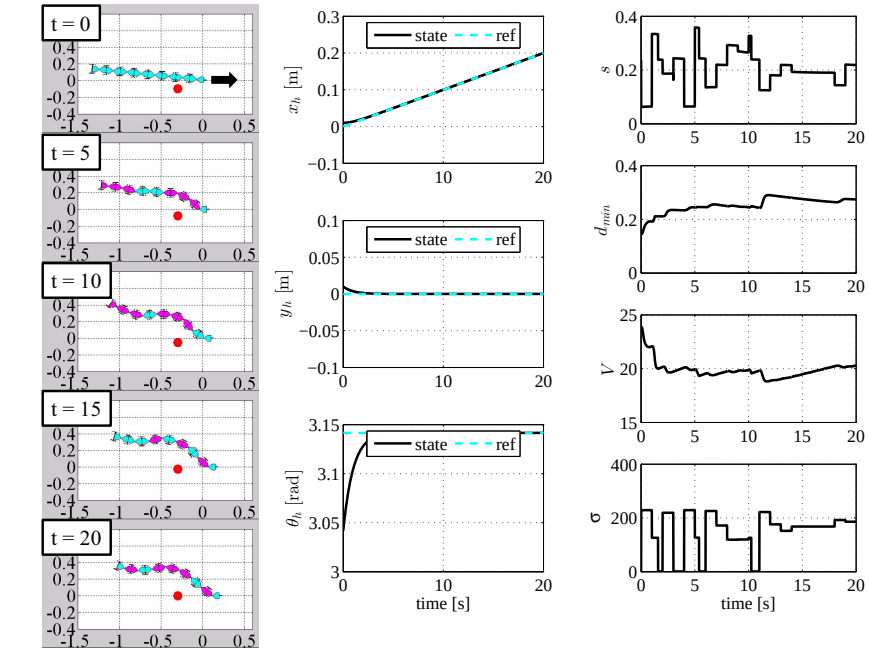

(a) Motions (b) $\boldsymbol{w}$ (c) s, d_{min}, V, and σ

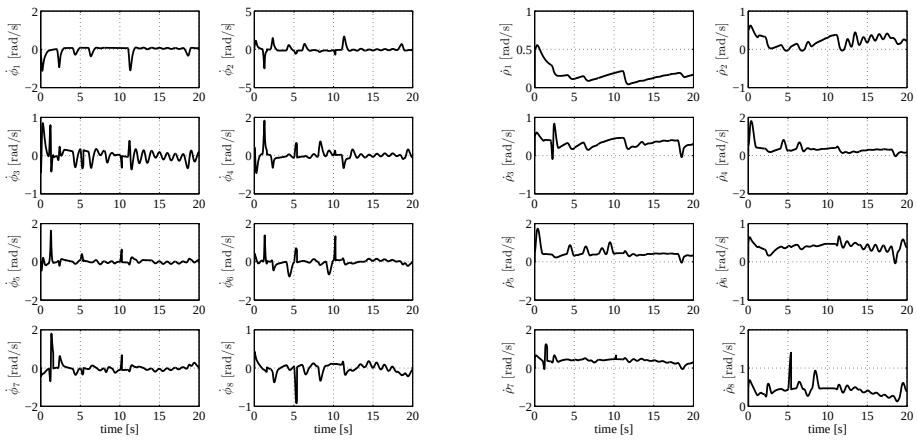

(d) $\dot{\boldsymbol{\phi}}$ (e) $\dot{\rho}$

Figure 8. Simulation results obtained using the smooth controller.

5. Experiments

Experiments were performed using the articulated mobile robot (Figure 11). Parameters of the robot were $n = 8$, $n_w = 8$, $l = 0.088$[m], $l_{w1} = l_{w3} = l_{w5} = l_{w7} = 0.052$[m], $l_{w2} = l_{w4} = l_{w6} = l_{w8} = -0.052$[m], and $r_w = 0.038$[m]. $\boldsymbol{w}$ and (x_{ob}, y_{ob}) were measured using an external motion capture system. The number of modes, as for simulations presented in Figure 9, was decreased to reduce the calculation cost. The parameter settings were $\boldsymbol{w}_d = [0.01t, 0, \pi]^T$, $\boldsymbol{K} = \boldsymbol{I}$, and $\Delta T = 2$[s].

Figure 12 shows the results obtained using the previous input (17) and $\kappa = -1$ (fixed value), and Figure 13 shows the results obtained using the proposed input (21) and $\kappa = \{\cos(2\pi t/\Delta T) - 1\}$. In both cases, $\boldsymbol{w}$ tracked the desired trajectory and the robot avoided a collision with the approaching human-operated moving obstacle. Whereas many jumps of input were generated in

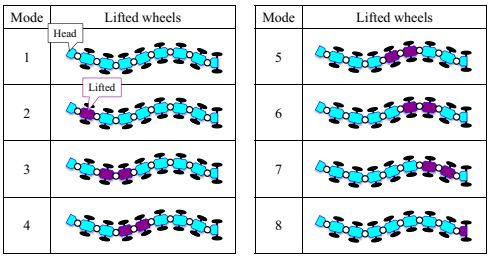

Figure 9. Relationship between reduced modes and lifted links.

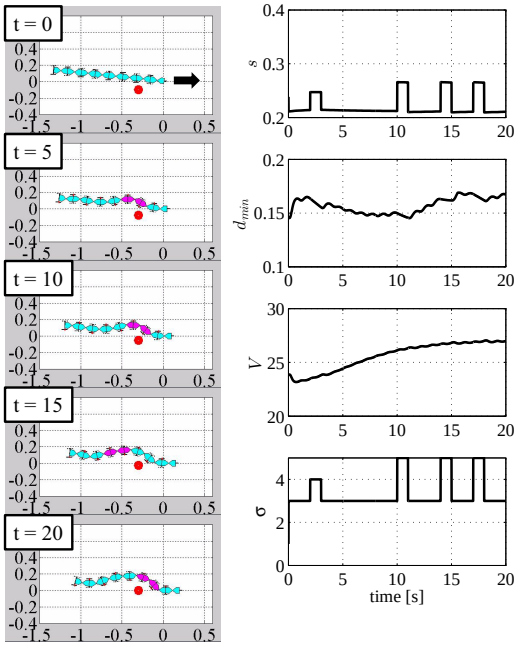

(a) Motions (b) s, d_{min}, V, and σ

Figure 10. Simulation results obtained using the smooth controller and reducing modes.

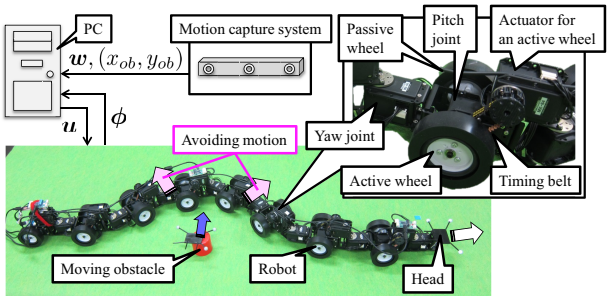

Figure 11. Articulated mobile robot and experimental system.

Figure 12(d) and (e), the input smoothly changed in Figure 13(d) and (e).

We thus demonstrated that the articulated mobile robot with active joints and active wheels can accomplish tracking of the head and avoidance of a moving obstacle using the proposed controller, and that the input is smoother than that of the previous work [16].

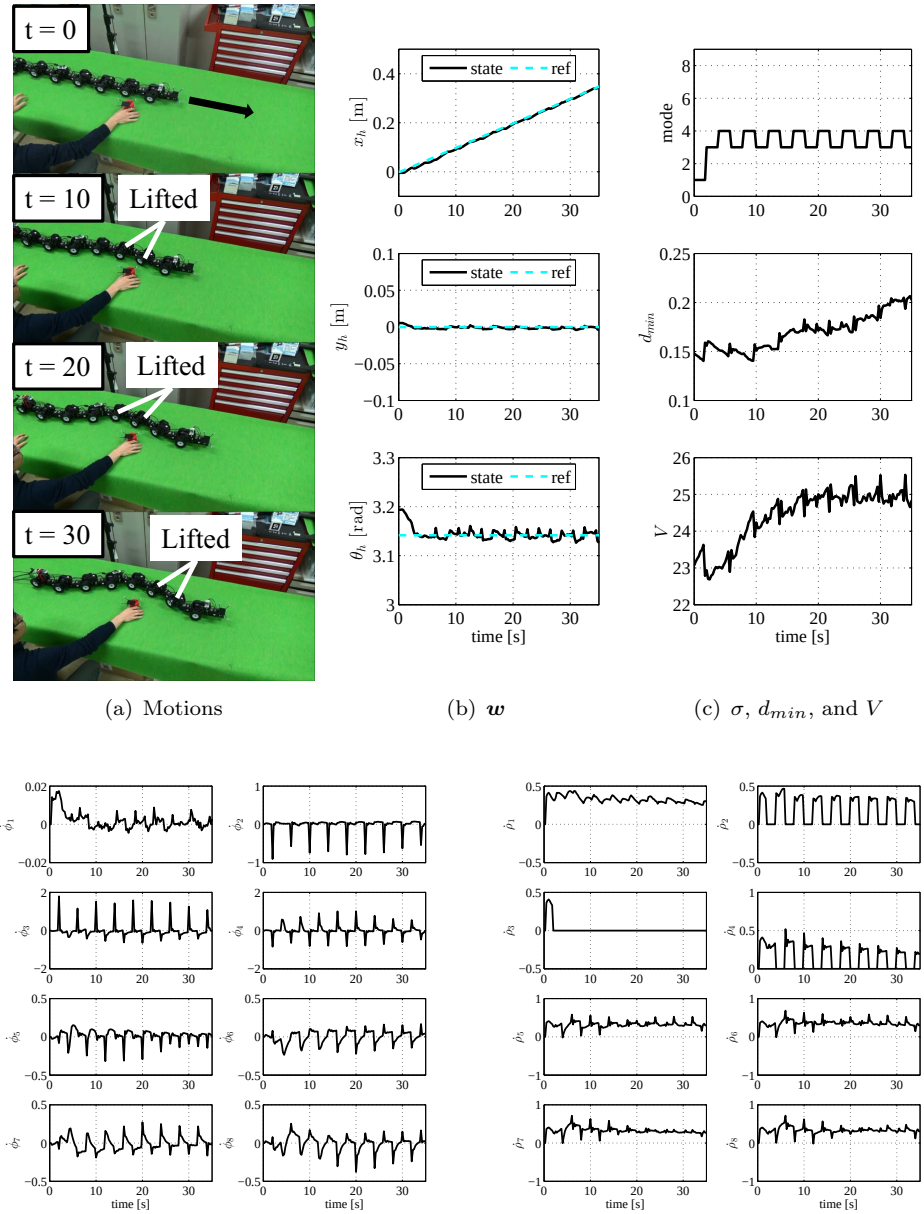

(a) Motions (b) $\boldsymbol{w}$ (c) σ, d_{min}, and V

(d) $\dot{\boldsymbol{\phi}}$ (e) $\dot{\rho}$

Figure 12. Experimental results obtained without using the smooth controller.

6. Conclusion

The paper described a smooth controller for an articulated mobile robot with switching constraints. A model of the robot introducing mode switching of the grounded/ungrounded wheels was derived. An improved control method that accomplishes both trajectory tracking and a subtask and generates smooth joint input at each switching time was proposed. Simulations and experimental results demonstrated the effectiveness of the proposed control method. Because a snake robot is a special case ($n_w = 0$) of the articulated robot considered in the present paper, the proposed smooth controller can be used for the snake robot.

The previous controller described in [16] required large torques to be applied to the joints and is unsuitable from the point of view of dynamics because the joint input (angular velocity) jumps at the switching time. In contrast, the smooth controller proposed in this paper prevents such

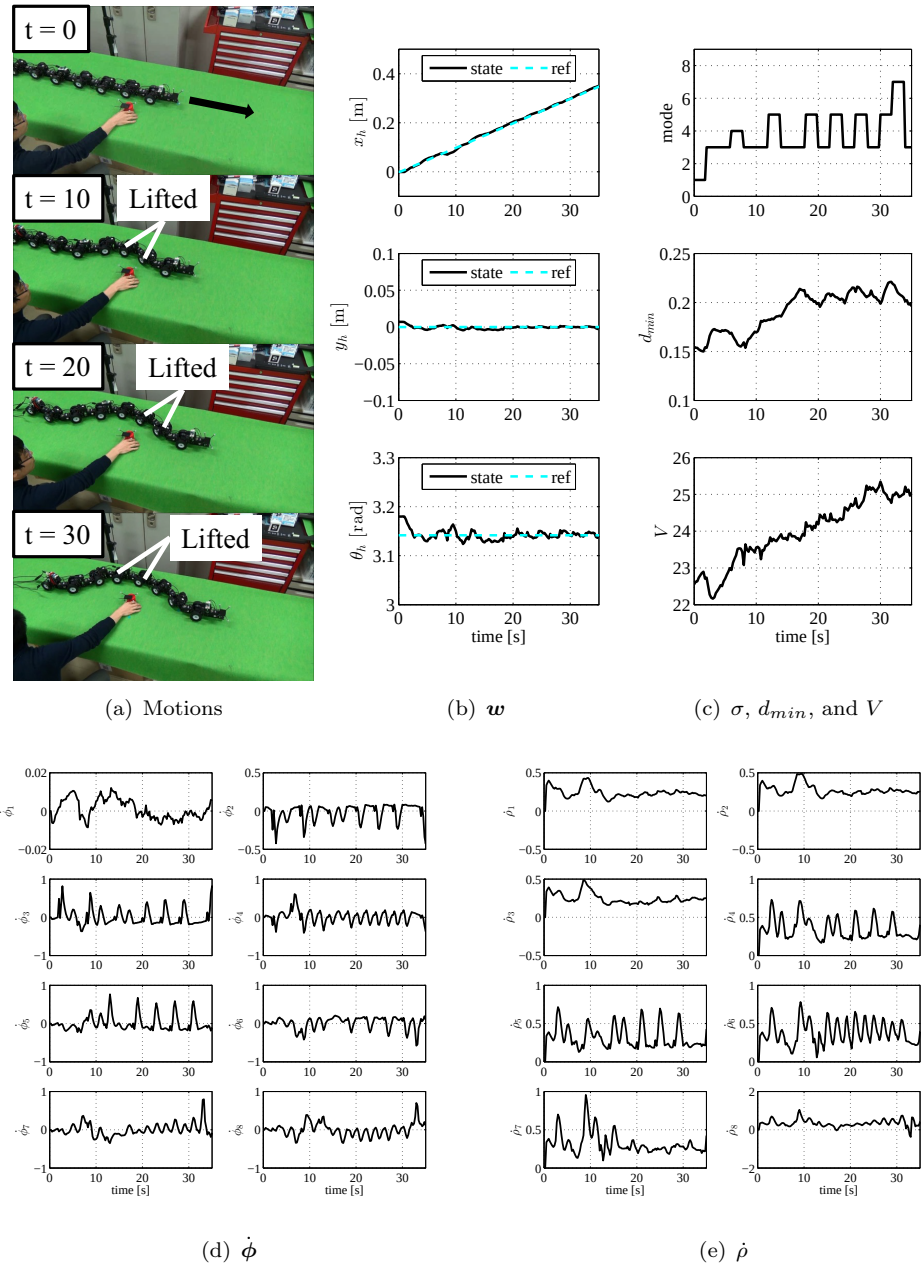

(a) Motions (b) $\boldsymbol{w}$ (c) σ, d_{min}, and V

(d) $\dot{\boldsymbol{\phi}}$ (e) $\dot{\rho}$

Figure 13. Experimental results obtained using the smooth controller.

torque during jumps in joint input. Hence, this controller, which is based on a dynamic model, could find application in future studies. In particular, integration with trajectory planning of the head of the robot, and application of the control method for complicated terrain, such as a step [10, 13, 28] or a cylindrical surface [7, 29], need to be addressed.

Acknowledgement

This work was partially supported by JSPS KAKENHI Grant Number 26870198, the Precise Measurement Technology Promotion Foundation, and the ImPACT Program of Council for Science, Technology and Innovation (Cabinet Office, Government of Japan).

References

[1] Granosik G. Hypermobile Robots – the Survey. J. of Intelligent and Robotic Systems; 2014; 75-1:147–169.

[2] Hirose S. Morishima A. Design and Control of a Mobile Robot With an Articulated Body. Int. J. Robotics Research; 1990; 9-2:99-113.

[3] Hirose S, Fukushima EF, Tsukagoshi S. Basic Steering Control Methods for The Articulated Body Mobile Robot. IEEE Control Systems Magazine; 1995; 15-1:5-14.

[4] Klaassen B, Paap KL. GMD-SNAKE2: A Snake-Like Robot Driven by Wheels and a Method for Motion Control. In: Proc. IEEE Int. Conf. on Robotics and Automation; 1999; Detroit, Michigan. p.3014-3019.

[5] Paap KL, Kirchner F, Klaassen B. Motion Control Scheme for a Snake-Like Robot. In: Proc. IEEE Int. Symp. on Computational Intelligence in Robotics and Automation; 1999; Monterey, CA. p.59-63.

[6] Kolesnik M, Streich H. Visual Orientation and Motion Control of MAKRO–Adaptation to the Sewer Environment. Proc. 7th Int. Conf. on Simulation of Adaptive Behavior on from animals to animats; 2002; Edinburgh, UK. p.62-69.

[7] Fjerdingen SA, Liljebäck P, Transeth AA. A snake-like robot for internal inspection of complex pipe structures. In: Proc. IEEE/RSJ Int. Conf. on Intelligent Robots and Systems; 2009; St. Louis, MO. p.5665-5671.

[8] Suzuki K, Nakano A, Endo G, Hirose S. Development of Multi-wheeled Snake-like Rescue Robots with Active Elastic Trunk. In: Proc. IEEE/RSJ Int. Conf. on Intelligent Robots and Systems; 2012; Algarve, Portugal. p.4602-4607.

[9] Osuka K, Kitajima H. Development of mobile inspection robot for rescue activities: MOIRA. In: Proc. IEEE/RSJ Int. Conf. on Intelligent Robots and Systems; 2003; Las Vegas, Nevada. p.3373-3377.

[10] Borenstein J, Hansen M, Borrell A. The OmniTread OT-4 Serpentine Robot – Design and Performance. J. of Field Robotics; 2007; 24-7:601-621.

[11] Kamegawa T, Yamasaki T, Igarashi H, Matsuno F. Development of the Snake-like Rescue Robot 'KOHGA'. In: Proc. IEEE Int. Conf. on Robotics and Automation; 2004; New Orleans, LA. p.5081-5086.

[12] Yamada H, Hirose S. Development of Practical 3-Dimensional Active Cord Mechanism ACM-R4. J. of Robotics and Mechatronics; 2006; 18-3: 305-311.

[13] Yamada H, Takaoka S, Hirose S. A snake-like robot for real-world inspection applications (the design and control of a practical active cord mechanism. Advanced Robotics; 2013; 27-1:47-60.

[14] Kouno K, Yamada H, Hirose S. Development of Active-Joint Active-Wheel High Traversability Snake-Like Robot ACM-R4.2. J. of Robotics and Mechatronics; 2013; 25-3:559-566.

[15] Murugendran B, Transeth AA, Fjerdingen SA. Modeling and Path-following for a Snake Robot with Active Wheels. In: Proc. IEEE/RSJ Int. Conf. on Intelligent Robots and Systems; 2009; St. Louis, MO. p.3643-3649.

[16] Tanaka M, Matsuno F. Control of Snake Robots with Switching Constraints: trajectory tracking with moving obstacle. Advanced Robotics; 2014; 28-6:415-429.

[17] Tanaka M, Tanaka K, Matsuno F. Approximate Path-Tracking Control of Snake Robot Joints with Switching Constraints. IEEE/ASME Trans. on Mechatronics; accepted.

[18] Tanaka M, Kon K, Tanaka K. Range-sensor-based Semi-autonomous Whole-body Collision Avoidance of a Snake Robot. IEEE Trans. on Control Systems Technology; accepted.

[19] Cole MOT. A class of low-pass FIR input shaping filters achieving exact residual vibration cancelation. Automatica; 2012; 48:2377-2380.

[20] Cole MOT., Wongratanaphisan T. A Direct Method of Adaptive FIR Input Shaping for Motion Control With Zero Residual Vibration. IEEE/ASME Trans. on Mechatronics; 2013; 18-1:316-327.

[21] Komoriya K., Tanie K. Trajectory Design and Control of a Wheel-type Mobile Robot Using B-spline Curve. In: Proc. IEEE/RSJ Int. Workshop on Intelligent Robots and Systems; 1989; Tsukuba, Japan. p.398-405.

[22] Fraichard T., Scheuer A. From Reeds and Shepp's to Continuous-Curvature Paths. IEEE Trans. on Robotics; 2004; 20-6:1025-1035.

[23] Yang K., Jung D., Sukkarieh S. Continuous curvature path-smoothing algorithm using cubic Bézier spiral curves for non-holonomic robots. Advanced Robotics; 2013; 27-4:247-258.

[24] Matsuno F, Mogi K. Redundancy controllable system and control of snake robots with redundancy based on kinematic model. In: Proc. IEEE Int. Conf. on Decision and, Control; 2000; Sydney, Aus-

tralia. p. 4791-4796.
[25] NakamuraY, Hanafusa H,Yoshikawa T. Task-priority based redundancy control of robot manipulators. Int. J. Robotic. Res. 1987; 6:3-15.
[26] Mayne DQ, Rawlings JB, Rao CV, Scokaert POM. Constrained model predictive control: Stability and optimality. Automatica; 2000; 36-6:789-814.
[27] Seguchi H, Ohtsuka T. Nonlinear receding horizon control of an underactuated hovercraft. Int. J. of Robust and Nonlinear Control; 2003; 13:381-398.
[28] Tanaka M, Tanaka K. Control of a Snake Robot for Ascending and Descending Steps. IEEE Trans. on Robotics; 2015; 31-2:511-520.
[29] Polchankajorn P, Maneewarn T. Development of a Helical Climbing Modular Snake Robot. In: Proc. IEEE Int. Conf. on Robotics and Automation; 2011; Shanghai, China. p.197-202.